Proceedings of the
44th IEEE Conference on Decision and Control, and
the European Control Conference 2005
Seville, Spain, December 12-15, 2005



# Real Time Modeling and Control in Plasma Arc Fabrication of Intermetallic Coatings

Marios Alaeddine, Rajesh Ranganathan, Teiichi Ando, and Charalabos C. Doumanidis

*Abstract*— **Successful fabrication of intermetallic coatings on surfaces of manufacturing interest involves regulation of the temperature/concentration dynamic distributions that develop in the molten layer during the thermal and reaction process. Modeling the spatio-temporal dynamics of this metallurgical process, however, requires partial differential equations that are cumbersome to solve on-line, as part of a real time reference model to the controller. To this end, we present a computationally parallel and meshless model to decipher the dynamics of the thermal coating process and to permit real time monitoring and control of the resulting coating microstructure. The analytical model, which is solved numerically using Matlab, is validated with nickel aluminide coatings processed on a robotic plasma arc laboratory station, through in-process infrared thermal sensing and off-line metallographic analysis. A proportional-integral control scheme, that involves on-line parameter identification and model adaptation, is also developed to facilitate the successful production of binary metal system coatings that exhibit the desired microstructure geometry and characteristics.**

## I. Introduction

INTERMETALLICS, such as those of nickel aluminides, have attracted much attention due to the superior properties they impart when applied as thin coating layers on surfaces of bulk parts. Today, the manufacturing industry makes use of nickel aluminides to reduce cavitation erosion in wear rings, water turbine buckets, diesel engine cylinder liners and pumps. Furthermore, due to their excellent dependability at elevated temperatures, nickel aluminides find use in internal combustion and jet engines, metal cutting, welding, aerospace applications, in repairing the dimensions of worn out high-temperature parts, and as interconnects in microelectronics [1]-[4].

M. Alaeddine was with the Thermal Manufacturing and Controls Laboratory at Tufts University, in Medford, MA 02155 USA. He is now with the Neurodynamics Laboratory at Children's Hospital, Harvard Medical School, Boston, MA 02115 USA (phone: 617-355-8310, fax: 617-730-0903/6, email: Marios.Alaeddine@childrens.harvard.edu).

R. Ranganathan and T. Ando are with the Department of Mechanical and Industrial Engineering, Northeastern University, Boston, MA 02115 USA (email: rajesh@coe.neu.edu, tando@coe.neu.edu).

C.C. Doumanidis is the founding director of the NanoManufacturing Program at the National Science Foundation, Arlington VA 22230 USA. He is now with the Department of Mechanical and Manufacturing Engineering, University of Cyprus, Nicosia, 1678 Cyprus (e-mail: cdoumani@ucy.ac.ucy).

Despite their technological significance in surface engineering, however, the processes that are presently used to produce nickel aluminides (e.g., plasma spraying, pack cementation, PVD, and CVD) result in coatings that exhibit poor bonding to the substrate, material porosity, structural coarsening due to bulk heat treatment, high capital cost of the equipment and/or low productivity [5], [6]. The manufacturing industry is therefore still in search for an economical, reliable, and controllable coating fabrication route with the ability to result in microstructures that impart the desired quality and safety to the thermally processed parts.

In order to address the aforementioned technological need, Ranganathan et al. presented a novel coating fabrication method based on in-situ thermal processing of layered elemental precursors [7]. In this technology, the precursors are prepared by electroplating a thin nickel layer on top of a substrate (e.g., steel) and then plating on top of that a thin aluminum layer using a proprietary commercial process [8], [9]. A plasma arc (PA) heat source of Gaussian power distribution scans the surface of the coating giving rise to the temperature evolution and component dissolution during the thermal melting and reaction process. Once the conditions in the molten/reaction layer increase sufficiently high for a nickel aluminide to nucleate, the nickel aluminide compound grows rapidly under the large chemical driving force to form an intermetallic coating layer on the surface (of the substrate) without melting the substrate itself.

In previous work, an analytical model of the PA coating fabrication method was developed and used to simulate the temperature/concentration dynamic distributions and microstructure growth that occur during the thermal process [10]-[12]. The model, which is computationally parallel and meshless (i.e., decoupled, with the capability to be solved numerically in real time), is based on kinetic growth theories, lumped energy and mass balances, and convolution expressions of distributed temperature and concentrations Green's fields (accounting for the orientation of their gradient and decomposing heat and mass transfer across the coating from substrate conduction). The numerical results were validated with Ni-Al coatings processed on a robotic plasma arc laboratory station, through in-process infrared thermal sensing and

0-7803-9568-9/05/$20.00 ©2005 IEEE

off-line metallographic analysis. It was shown that the predicted coating temperature, dissolution penetration value, and thickness of the coating layer compare well with the experimentally obtained results, therefore supporting the model as a real time basis for design and/or adaptation of a thermal control system for the coating process.

In this paper, a Monte-Carlo sample control method, which consists of on-line parameter identification and model adaptation laws, is developed for in-process estimation and control of the coating microstructure that is obtained during the thermal and reaction process. A control-input simulation is conducted to demonstrate the successful performance of the method.

## II. Mathematical Model Developement

As a coating element of surface dimensions ($\Delta y$, $\Delta z$) which are comparable to its thickness dimension $\Delta x$ (= 30 μm in the experiments) starts to interact with the approaching power density distribution of the heat source (PA distribution diameter = 3 mm, based on PA specifications) it starts to experience an increase in temperature. Once the temperature of the element reaches the melting temperature of Al, the Al layer starts to melt absorbing the respective energy supplied by the heat source in order to undergo the phase change. It should be noted that the melting front surface follows tangentially the local isotherm $T$ surface (see figures 1, 2.a) oriented at angles θ and φ with respect to the $y$ and $z$ axes, respectively (angles θ and φ can be determined at all times by the slope of the computed gradient of the conduction field with respect to the normal directions $x$ and $y$) [12].

Once the melting Al front touches the solid Ni interface (figure 2.b), a temperature-dependent Ni dissolution into the molten region starts to occur together with the gradual melting of the remaining Al layer (figure 2.c). The element's rate of change of energy can be described as:

$$\begin{aligned}
&\dot{q}_i(t) - \left[\dot{q}_o(t) + \dot{q}_c(t) + \dot{q}_l(t)\right] = \\
&\bar{x}(t)\left(\rho_{\substack{Al\\liq}}\frac{\bar{x}_{Al}(t)}{\bar{x}(t)} + \rho_{\substack{Ni\\liq}}\frac{\bar{x}(t)-\bar{x}_{Al}(t)}{\bar{x}(t)}\right) \\
&\qquad\left(c_{\substack{Al\\liq}}\frac{\bar{x}_{Al}(t)}{\bar{x}(t)} + c_{\substack{Ni\\liq}}\frac{\bar{x}(t)-\bar{x}_{Al}(t)}{\bar{x}(t)}\right)\frac{dT}{dt} \\
&+\left\{\left(l_{Al}-\bar{x}_{Al}(t)\right)\rho_{\substack{Al\\sol}}c_{\substack{Al\\sol}}\frac{dT}{dt}\right\} \\
&\quad+\left(l_{Ni}-\left(\bar{x}(t)-\bar{x}_{Al}(t)\right)\right)\rho_{\substack{Ni\\sol}}c_{\substack{Ni\\sol}}\frac{dT}{dt} \\
&\qquad+\left\{\rho_{\substack{Al\\sol}}\Delta h_{Al}\frac{d\bar{x}_{Al}}{dt}\right\}+\rho_{\substack{Ni\\sol}}\Delta h_{Ni}\frac{d\bar{x}_{Ni}}{dt}
\end{aligned} \tag{1}$$

where $\dot{q}_i$ represents the rate of supply of energy density into the element from the heat source (W/m$^2$), $\dot{q}_o$ the rate at which heat is lost and conducted into the steel substrate (W/m$^2$), $\dot{q}_c$ the rate of lateral heat exchange to the surrounding coating (W/m$^2$), $\dot{q}_l$ the rate at which heat is lost to the surroundings due to convection and radiation at the coating surface (W/m$^2$), $\rho$ the material density (kg/m$^3$), $c$ the specific heat capacity (J/kgK), $l$ the length (along the $x$-axis) of the element (m), and finally $T$ the coating temperature (K) at location ($y$, $z$).

Furthermore, $\Delta h_{Al}$ and $\Delta h_{Ni}$ denote the latent heat of fusion of aluminum and nickel, respectively, in (J/kg). Finally, $\bar{x}(t) = \bar{x}_{Al}(t) + \bar{x}_{Ni}(t)$ denotes the "equivalent position" of the melting front across the thickness of the coating, (where $\bar{x}_{Al,\,Ni}(t) = V^{Al,\,Ni}_{molten}(t)\big/A$, i.e., the molten volume of Al and Ni, respectively, divided by the cross-sectional area of the element).

This stage of the process continues until the point of complete Al melting is reached (figure 2.d). Dissolution of pure Ni into the melt continues to occur from this point on. In turn, this stage of pure Ni dissolution continues until the temperature in the coating layers reaches a maximum. It should be noted that the stage of pure Ni dissolution (figure 2.d.), as well as the heating up and pure melting of Al (figure 2.a) can be expressed as simplified particular solutions of (1) [10].

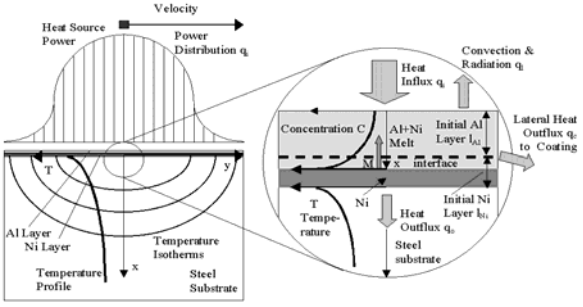


Fig 1. Thermal processing of the Ni-Al coating.

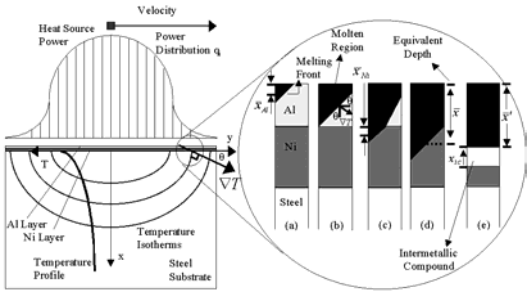


Fig. 2. Front view of an element located at the center of the heat source trajectory as it undergoes thermal processing, i.e., ($y$=$Y(t)$, $z$=0).

Once the temperature/concentration conditions in the molten layer increase sufficiently high to permit the nucleation of a nickel aluminide compound, the nickel aluminide grows very rapidly under the large chemical driving force to cause rapid solidification of the molten Ni-Al layer. This stage of the process (shown in figure 2.e) can be expressed as:

$$\left[\dot{q}_i(t)+\left\{\rho_{ic}\Delta h_{ic}\frac{dx_{ic}}{dt}\right\}\right]-\left[\dot{q}_o(t)+\dot{q}_c(t)+\dot{q}_l(t)\right]=$$
$$\bar{x}(t)'\left(\rho_{\substack{Al\\liq}}\frac{l_{Al}'}{\bar{x}(t)'}+\rho_{\substack{Ni\\liq}}\frac{l_{Ni}'}{\bar{x}(t)'}\right)\left(c_{\substack{Al\\liq}}\frac{l_{Al}'}{\bar{x}(t)'}+c_{\substack{Ni\\liq}}\frac{l_{Ni}'}{\bar{x}(t)'}\right)\frac{dT}{dt}$$
$$+x_{ic}(t)\rho_{ic}c_{ic}\frac{dT}{dt}+\left(l_{Ni}-\left(\bar{x}(t)-l_{Al}(t)\right)\right)\rho_{\substack{Ni\\sol}}c_{\substack{Ni\\sol}}\frac{dT}{dt} \quad (2)$$

where $\rho_{ic}$, $c_{ic}$, and $\Delta h_{ic}$ represent the material density (kg/m$^3$), the specific heat (J/kgK), and the latent heat of fusion of the intermetallic compound (J/kg), respectively, $x_{ic}$ the thickness of the solidified compound (in (m)) with reference to the interface of the remaining solid nickel (see figure 2.e), $l_{Al}$' and $l_{Ni}$' the length (in (m)) that corresponds to the mass of Al and Ni that remains in the molten region, respectively, and $\bar{x}(t)'=\bar{x}(t)-x_{ic}(t)$ denotes the new interface position of the molten aluminum-nickel region across the thickness of the coating.

The energy balance of the coating in the previous process stages yields ordinary differential equations, that can be integrated numerically (e.g., by a Runge-Kutta 45 routine) for the coating temperature $T(t)$, when the following variables are known: 1) the heat fluxes lost from the coating element to the substrate $\dot{q}_o$, the surface $\dot{q}_l$ and the surrounding coating $\dot{q}_c$, 2) the "equivalent position" of the melting front in reference to the thickness of the coating, and 3) the position of the solidifying interface $x_{ic}$. In the following sections, ways to obtain these unknowns are presented in a summarized form. A more detailed discussion/derivation of the equations can be found in [10]-[12].

### *A. Heat Transfer in the Coating Layers*

The lateral heat flux to the surrounding coating is obtained by an energy balance across the sides of the element:

$$\dot{q}_c(y,z;t)=\left[K_{Al}l_{Al}+K_{Ni}l_{Ni}\right]*\nabla^2T(0,y,z;t) \quad (3)$$

and the heat loss flux because of convective and radiative cooling at the element's surface is

$$\dot{q}_l(y,z;t)=h\left[T(0,y,z;t)-T_\infty(t)\right]+\varepsilon(y,z)b\left(T^4(0,y,z;t)-T_\infty{}^4(t)\right) \quad (4)$$

where $T_\infty$ is the ambient temperature of the PA gas (K), $h$ the convective heat transfer coefficient (W/m$^2$K), $\varepsilon$ the surface emissivity, and $b$ the Boltzmann constant (W/m$^2$K$^4$).

### *B. Thermal Conduction in the Substrate*

The power influx distribution applied to the substrate during the process gives rise to a temperature field that can be computed by the convolution of the power influx distribution with the Green's function over the coating surface area. Taking into account the non-stationary position of the heat source on the surface of the precursor, it can be shown that the temperature that develops on the surface of the substrate is [10], [13]:

$$T(t)=T(0,y,z;t)=T(0,y,z;0)+$$
$$\int_0^t\frac{4\pi\sigma^2\dot{q}_o(\psi,\zeta;\tau)\Big/\left(2\sigma^2+4\alpha_s(t-\tau)\right)}{\left(\rho_sc_s\pi\sqrt{4\pi\alpha_s(t-\tau)}\right)\exp\left[-\frac{(\psi-Y(t))^2+(\zeta-Z)^2}{2\sigma^2}\right]}$$
$$\sum_{j=-\infty}^{\infty}\exp\left[-\frac{(y-Y(\tau))^2+(z-Z(\tau))^2}{2\sigma^2+4\alpha_s(t-\tau)}+\frac{(2jL)^2}{4\alpha_s(t-\tau)}\right]d\tau \quad (5)$$

where $\sigma$ denotes the distribution radius of the source, $(\psi, \zeta)$ the location/coordinate values (in the $y$ and $z$ axes, respectively) of the examined surface element, and $(Y(t), Z)$ those of the traveling source [14]. Furthermore, $\rho_s$ and $c_s$ denote the density and specific heat of the substrate, respectively, $L$ the substrate thickness, and $\alpha_s=K_s/\rho_sc_s$ the thermal diffusivity (of the substrate) in (m$^2$/s).

When the temperature of the substrate surface is equated to that resulting from the energy balance equations (of the coating) in successive time steps $\Delta t$, the magnitude of the Gaussian power influx distribution $\dot{q}_o$ can be obtained by deconvolution from (5).

### *C. Nickel Dissolution in the Molten Region*

The mass influx of nickel into the melt during the dissolution stage of the process generates a concentration field that can be computed by the convolution of the mass influx distribution with the diffusive Green's function over time $t$. This results in [10]:

$$C(\bar{x},t)=\int_0^t g\left(\bar{x}(t)-\chi(\tau);t-\tau\right)\rho_{\substack{Ni\\sol}}\frac{d\bar{x}_{Ni}}{dt}(\chi,\tau)d\tau\equiv C(t) \quad (6)$$

where $g$ denotes the diffusive Green's function, i.e., the concentration at interface "equivalent position" $\bar{x}$ at time $t$

because of a unit mass influx of Ni (1 kg/m$^2$) at a previous solid-liquid interface location $\chi$ at time $\tau$ [15]. Furthermore, $C(t)$ in units of (kg/m$^3$) is the Ni concentration in the melt at the interface, which is related to the local temperature by the liquidus curve of the metastable Ni-Al phase diagram [16], thus allowing numerical deconvolution (in time steps $\Delta t$) of (6) for the "equivalent position" of the Ni interface during the dissolution stage of the process. Of note, at the stage of the process where Ni dissolution and melting of Al occur simultaneously, it can be shown that the "equivalent position" of the melting Al interface is related to the concentration of Ni in the melt by [10]:

$$\bar{x}_{Al} = \int_0^{\bar{x}(t)} \left(1 - \frac{C(x,t)}{\rho_{\substack{Ni \\ sol}}}\right) dx \qquad (7)$$

### *D. Intermetallic Compound Growth*

The growth rate of the nickel aluminide, $dx_{ic}/dt$, is governed by the driving force across the liquid-nickel aluminide interface, $-\Delta G$ (J/mol), and is obtained by:

$$v = -v_o \left(\frac{\Delta G}{RT}\right) \equiv \frac{dx_{ic}}{dt} \qquad (8)$$

where $R$ is the gas constant (J/molK), $v_o$ the maximum crystallization velocity (m/s) of the compound, and $T$ the interface temperature (K). $\Delta G$ (at the interface temperature $T$) is dependent on the compound composition ($Ni_2Al_3$, NiAl, etc) and the solute (Ni) concentration at the solidifying compound-molten layer interface, as discussed in detail in [11], [12].

## III. Model Implementation in Laboratory Tests

Thermal processing experiments are performed using a robotic plasma arc welding station shown in figure 3. The welding setup includes a water-cooled plasma arc torch, powered by a solid state DC-AC welding transformer rated at 300 A through a plasma console, and operated in the transferred arc, alternate current (AC) mode. Argon ($Ar+2\%O_2$) is employed as both the plasma and the inert shielding gas at a flow rate of 0.4 LPM at STP. The plasma torch is guided by a 6-DOF articulated robot arm hardened to PA electromagnetic interference, with a positioning repeatability of 50 μm.

During the experiments, an infrared pyrometry camera monitors the temperature distribution on the top surface of the thermally-processed part. The camera consists of a stationary electromechanical galvanometer scanner and a liquid nitrogen-cooled HgCdTe detector, sensitive in the wavelength range of 8-12 μm. Such a non-contact temperature measuring method offers the advantage of no interference with both the temperature field of the specimen and the moving PA torch. The temperature data obtained by the camera are recorded during the test in standard composite video format and analyzed off-line using a frame grabber and thermal image processing software. It should be noted that since the camera actually measures infrared emission, the emissivity value of the specimen surface is required for temperature conversion. This was obtained by off-line comparative thermometry tests using k-type thermocouples and found to be $\varepsilon = 0.5$ [10].

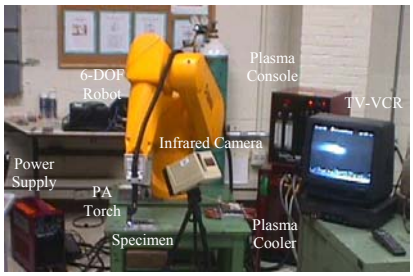


Fig. 3. Plasma arc welding station.

Several experiments were conducted in the laboratory using different heat input rates and heat source traverse rates. The resulting microstructures were investigated (off-line) using scanning electron microscopy. In order to shed light on the thermo-material dynamics that led to the resulting microstructures, several simulations were conducted using the developed model. It was shown that the simulation results for the coating temperature, melt interface motion, and thickness of the resulting coating layer were in good agreement with experimental results [10]-[12]. An example of these results is shown below for a heat input rate of 880 (W) and a heat source traverse rate of 9 (mm/s).

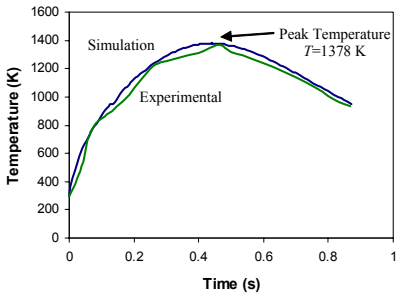


Fig. 4. Simulated and experimental (actual) temperature variation in an element located at ($y$=3 mm, 0).

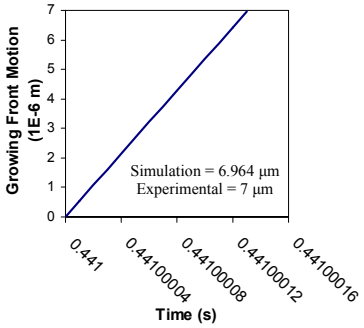


Fig. 5. Thickness of the resulting $Ni_2Al_3$ coating layer.

Plots of the simulated interface motion of the melting Al and dissolving Ni layers were also compared to the experimentally obtained depth of melting and were found to be in good agreement [10]-[12].

## IV. Control of the Intermetallic Compound Composition and Thickness

With the model able to successfully simulate the dynamics of the above-described coating fabrication method, a control scheme can now be developed for real time monitoring and control of the intermetallic compound composition ($Ni_2Al_3$, NiAl, etc) and coating layer thickness obtained during the thermal/reaction process. For the control scheme to be efficient and applicable in real time, instead of simulating the full temperature/concentration distributions and coating thickness $x_{ic}$ over the entire coating layer ($y$, $z$), these outputs are evaluated only at distinct sample positions ($y_i$, $z_i$), for $i$ = 1 to $N$. With the field of view (FOV) of the infrared camera moving along with the traversing PA heat source, the sampled elements appear as moving locations ($y_i(t)$, $z_i$) in the FOV coordinate system shown in figure 6.

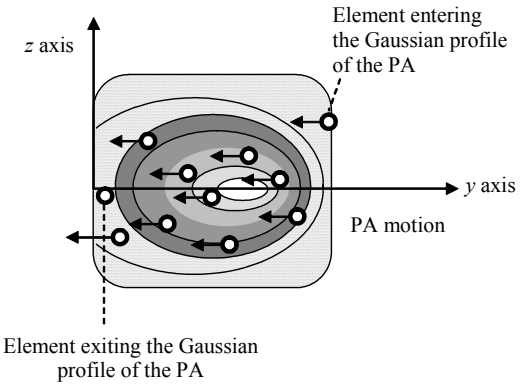


Fig. 6. Schematic of a Monte-Carlo sample control method.

Sampled locations are dynamically defined at one horizontal end of the FOV (figure 6) by random choice of the vertical coordinate (i.e., by a Gaussian selection of $z_i(\tau)$), and are followed as they undergo thermal processing. When each moving location exits the PA heat source a prediction of the local/geometric final microstructure has been estimated by the model and is available for in-process control. Furthermore, the temperature values predicted by the model at the $N$ sampled locations are compared (in time steps $\Delta t_c$) to the ones obtained by the infrared camera. This comparison between the actual and model-predicted temperature values allows for in-process parameter identification and real time model adaptation. The control scheme, seen in block diagram notation in figure 7, is described in the following sections.

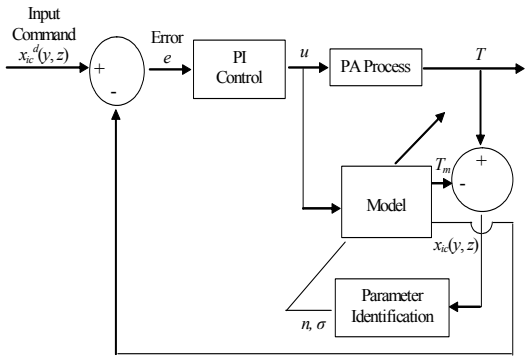


Fig. 7. Model-reference control scheme.

### A. Identification of the Efficiency of the Heat Source

The efficiency $n$ of the PA heat source can be related to the temperature error obtained at each sampled location by an integral adaptation law of the form:

$$\dot{n} = \frac{dn}{dt} = \gamma_1 \sum_{i=1}^{N} e_i \tag{9}$$

where $\gamma_1$ is a proportional gain, and $e_i$ (= $T$- $T_{mi}$) the error between the actual and model-predicted temperature values ($T$ and $T_m$, respectively) at each sampled location $i$.

### B. Identification of the Gaussian Distribution Radius of the Heat Source

The Gaussian distribution radius $\sigma$ of the heat source dictates (in a quasi-linear approximation) the curvature of the temperature distribution formed by the $N$ sampled elements. It is therefore estimated/identified by an integral adaptation law of the form:

$$\dot{\sigma} = \frac{d\sigma}{dt} = \gamma_2 \sum_{i=1}^{N} r_i \left( \bar{T} - T_{mi} \right) e_i \tag{10}$$

where $\gamma_2$ is a proportional gain, and $\bar{T}$ the average temperature value of the $N$ sampled elements. Furthermore, $r_i$ denotes the distance of each sampled location ($y_i(t = j\Delta t_c)$, $z_i$) from the center of the PA heat source/temperature distribution ($y = 0, z = 0$), i.e., $r_i = \sqrt{y_i(t)^2 + z_i^2}$ .

### C. Proportional-Integral Control

Once the parameters ($n$ and $\sigma$) of the PA heat source have been identified, the model-predicted coating thickness at the sampled locations can be used for in-process control. The controller, which involves an error-based proportional-integral (PI) law, can be expressed by:

$$u(t) = K_P E(t) + K_I \int_0^t E(\tau) d\tau \tag{11}$$

where $u$ denotes the power of the PA heat source (W), $K_P$ and $K_I$ the proportional and integral control gains, respectively, and $E$ the state error.

### D. Control-Input Simulation

Having identified $n$ and $\sigma$ of the PA heat source (using (9) and (10) in conjunction with experimental measurements), a simulation is conducted where it is desired to obtain a $Ni_2Al_3$ coating layer of an average thickness of 3 μm along the diameter ($z$-axis) of the PA heat source. This is shown graphically in figure 8. In the same figure, the control-input behavior is observed at time steps $t_c = \Delta t_c$ (= 0.85 s), … , $8\Delta t_c$ (i.e., the time equivalent to the duration of an actual experiment). The controller-generated power inputs used to obtain the respective coating thicknesses are provided in figure 9. Furthermore, figure 10 shows the average coating thickness error obtained during the duration of the simulation.

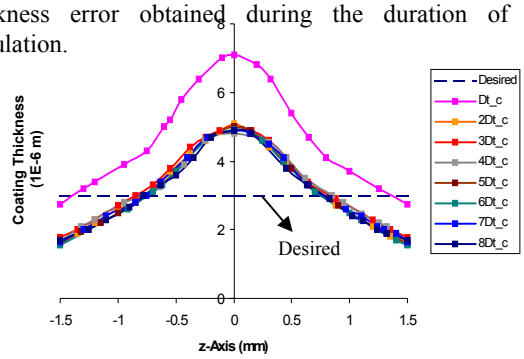


Fig. 8. Desired and controller-generated $Ni_2Al_3$ coating thickness.

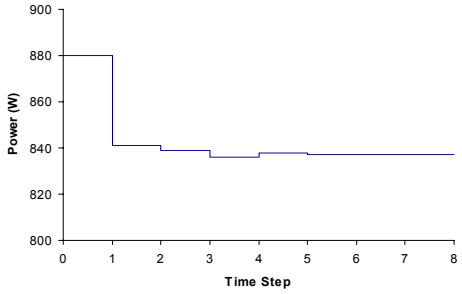


Fig. 9. Controller-generated power inputs.

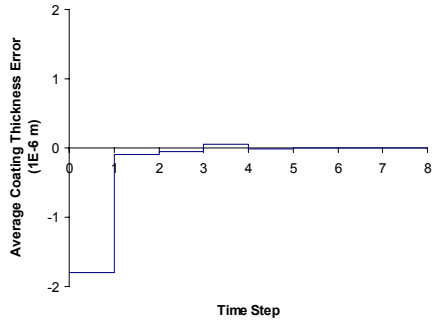


Fig. 10. Average coating thickness error.

## V. Conclusion

This paper addressed the need of modeling and control of the microstructure growth that occurs during production of intermetallic coatings. An analytical model was developed, based on principles of heat/mass transfer and kinetic growth theories, to decipher the spatio-temporal dynamics of the coating fabrication process. Following the validation of the model with experimental results (obtained using a robotic plasma arc welding station), a control method was developed using the model as a real time *observer* for in-process monitoring and regulation of the microstructure geometry and composition.

## References


[1] Sugama, T., 1998, "Polyphenylenesulphide-sealed Ni-Al Coatings for Protecting Steel from Corrosion and Oxidation in Geothermal Environments," *Journal of Material Science*, Vol. 33, pp. 3791-3803.

[2] ASM Handbook, 1990, *Friction, Lubrication and Wear Technology*, Vol. 18, American Society for Metals, Metals Park, OH.

[3] Ng, H.P., Meng, X.K., and Ngan A.H.W., 1998, "An Investigation into the Fabrication and Properties of $Ni_3Al$ Thin Coatings on Nickel Substrates," *Scripta Materialia*, Vol. 39, pp. 1737-1742.

[4] Pope, D.P., and Darolia, R., 1996, "High-Temperature Applications of Intermetallic Compounds," *Journal of Material Education*, Vol. 18, pp. 205-219.

[5] Bunshah, R.F., (editor), 1994, *Handbook of Deposition Technologies for Films and Coatings*, *2nd Edition*, Noyes Publications, Park Ridge, NJ.

[6] Goward, G.W., Boone, D.H., and Giggins, C.S., 1967, "Formation and Degradation Mechanisms of Aluminide Coatings on Nickel-Base Superalloys," *ASM Transactions*, Vol. 60, pp. 228-241.

[7] Ranganathan, R., Vayena, O., Doumanidis, C.C., Ando, T., Blue, C., 2001, "In-situ Processing of Nickel Aluminides," *Proceedings of the 2001 Minerals, Metals and Materials Society Annual Meeting*, pp. 171-180.

[8] Fromberg, W., and Donaldson, F.A.S., 1996, "Electroplating with Aluminum," *Advanced Materials and Processes*, Vol. 2, pp. 33-35.

[9] Fischer, J., and Fuhr, B., 1999, "Aluminum Plating Replaces Cadmium," *Advanced Materials Processes*, Vol. 155, pp. 27-29.

[10] Alaeddine, M., Ranganathan, R., Ando, T., Doumanidis C.C., 2004, "Modeling the Melting and Dissolution Stages During Reactive Thermal Processing of Intermetallic Coatings from Layered Precursors," *ASME Journal of Manufacturing Science and Engineering* (in press).

[11] Alaeddine, M., Ranganathan, R., Ando, T., Doumanidis C.C., 2004, "Modeling the Intermetallic Coating Growth During Reactive Thermal Processing of Layered Precursors," *Surface and Coatings Technology* (submitted).

[12] Alaeddine, M., 2004, "Meshless Modeling and Control of the Reactive Fabrication of Intermetallic Coatings from Layered Precursors," Ph.D. Dissertation, Department of Mechanical Engineering, Tufts University.

[13] Tsai, N.S., and Eagar, T.W., 1984, *Modelling of Casting and Welding Processes II*, Dantzig, J.A., and Berry, J.V., (editors), AIME Vol. 317, NY.

[14] Doumanidis, C.C., and Fourligkas, N., 1996, "Distributed Parameter Control of the Heat Source Trajectory in Thermal Materials Processing," *ASME Journal of Manufacturing Science and Engineering*, Vol. 118, pp. 571-578.

[15] Carslaw, H.S., and Jaeger, J.C., 1959, *Conduction of Heat in Solids*, *2nd Edition*, Oxford, Clarendon Press.

[16] Ranganathan, R., 2001, *Fabrication of Intermetallic and Composite Coatings from Precursors*, Masters Thesis, Northeastern University, Boston, MA.